Inorganic Chemistry

ARTICLE

pubs.acs.org/IC

Synthesis, Characterization, and Catalase Activity of a Water-Soluble diMn^{III} Complex of a Sulphonato-Substituted Schiff Base Ligand: An Efficient Catalyst for H_2O_2 Disproportionation

Claudia Palopoli,[†] Natalia Bruzzo,[†] Christelle Hureau,[‡] Sonia Ladeira,[‡,§] Daniel Murgida,[⊥] and Sandra Signorella*[,†]

[†]Departamento de Química Física/IQUIR-CONICET, Facultad de Ciencias Bioquímicas y Farmacéuticas, Universidad Nacional de Rosario, Suipacha 531, S2002LRK Rosario, Argentina

[‡]CNRS, LCC (Laboratoire de Chimie de Coordination), 205, route de Narbonne, F-31077 Toulouse, France and Université de Toulouse, UPS, INPT, LCC, F-31077 Toulouse, France

[§]Institut de Chimie de Toulouse, FR2599, 118 route de Narbonne, F-31062 Toulouse, France

[⊥]Departamento de Química Inorgánica, Analítica y Química Física/INQUIMAE-CONICET, Facultad de Ciencias Exactas y Naturales, Universidad de Buenos Aires, Ciudad Universitaria, Pabellón 2, Buenos Aires C1428EHA, Argentina

Supporting Information

ABSTRACT: A new diMn^{III} complex, Na[Mn_2(3-Me-5-SO_3-salpentO)(μ-MeO)(μ-AcO)(H_2O)]·4H_2O (**1**), where salpentOH = 1,5-bis(salicylidenamino) pentan-3-ol, was synthesized and structurally characterized. The complex possesses a bis(μ-alkoxo)(μ-acetato) triply bridged diMn^{III} core, the structure of which is retained upon dissolution. Complex **1** is highly efficient to disproportionate H_2O_2 in an aqueous solution of pH ≥ 8.5 or in DMF, with only a slight decrease of activity. Electrospray ionization mass spectrometry, EPR, and UV−vis spectroscopy used to monitor the H_2O_2 disproportionation in buffered basic medium, suggest that the major active form of the catalyst during cycling occurs in the Mn^{III}_2 oxidation state and that the starting complex retains the dinuclearity and composition during catalysis, with the acetate that moves from bridging to terminal ligand. UV−vis and Raman spectroscopy of H_2O_2 + **1** + Bu_4NOH mixtures in DMF suggest that the catalytic cycle involves Mn^{III}_2/Mn^{IV}_2 oxidation levels. At pH 10.6 in an Et_3N/Et_3NH^+ buffer, complex **1** catalyzes dismutation of H_2O_2 with saturation kinetics on the substrate, first order dependence on the catalyst, and k_{cat}/K_M = 16(1) × 10^2 s^{-1} M^{-1}. During catalysis, the exogenous base contributes to retain the integrity of the bis(μ-alkoxo) doubly bridged diMn core and favors the formation of the catalyst−peroxide adduct (low value of K_M), rendering **1** a highly efficient catalyst for H_2O_2 disproportionation.

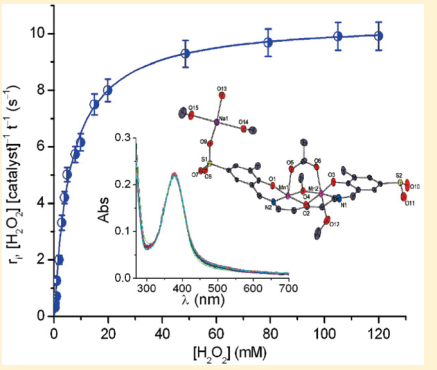

INTRODUCTION

Catalases (CATs) protect biological systems against oxidative damage caused by hydrogen peroxide generated during aerobic metabolism through bielectronic reduction of molecular oxygen.[1] In a variety of pathological situations, the production of peroxide overwhelms the activity of endogenous defense systems and results in cell damage.[2] In this context, the development of low molecular weight CAT mimics as therapeutic agents have been actively sought for the prevention of oxidative stress injuries,[3] and Mn-based catalytic antioxidants have shown beneficial effects against oxidative stress in vivo.[4] MnCATs are a group of enzymes that catalyze disproportionation of intracellular H_2O_2 into H_2O and O_2 by using a Mn_2(μ-O_2CR)(μ-O/OH/H_2O)$_2$ structural unit as the active site.[5] To mimic this metallosite, it is essential to employ ligands that reproduce the singularities of the metal environment in the biosite as well as the electronic properties that control catalysis. A number of dinuclear manganese-based complexes have been investigated as low-molecular-weight catalytic scavengers of H_2O_2.[6−19] However, most of the tested complexes are not soluble in water or lose activity in aqueous media.[15−19] Therefore, there is a need to design efficient catalytic antioxidants with improved stability in aqueous media to be useful as drugs.

We report here the synthesis, structure, properties, and catalase-like activity of a new water-soluble Mn^{III}_2 complex: Na[Mn_2(3-Me-5-SO_3-salpentO)(μ-OAc)(μ-OMe)(H_2O)]·4H_2O (**1**), where 3-Me-5-SO_3-salpentOH = 1,5-bis(3-methyl-5-sulphonatosalicylideneamino)pentan-3-ol. Further, we check the CAT activity in protic and nonprotic solvents and determine the

Received: May 28, 2011
Published: August 22, 2011

Scheme 1. Synthesis of Na_2[3-Me-5-SO_3-salpentOH]

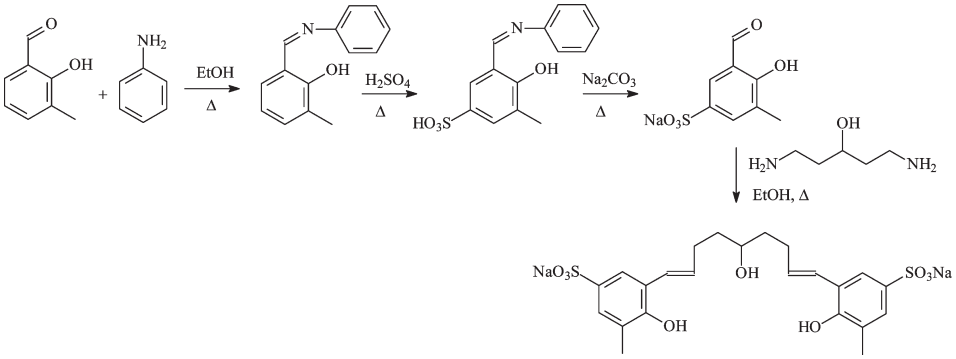

effect of an exogenous base on the catalyst stability in aqueous medium.

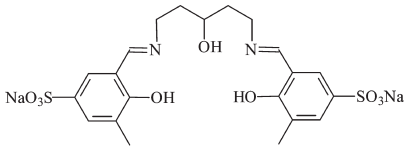

Na_2[3-Me-5-SO_3-salpentOH]

EXPERIMENTAL SECTION

Materials. All reagents or AR chemicals were used as purchased. Solvents were purified by standard methods. The concentration of the H_2O_2 stock solution was determined by iodometric titration.

Synthesis of the Ligand. Na_2[3-Me-5-SO_3-salpentOH] was synthesized through the reaction sequence shown in scheme 1.

Sodium 3-methylsalicylaldehyde-5-sulfonate was prepared through a synthetic procedure adapted from references.[20a,20b] A mixture of 3-methyl-2-hydroxybenzaldehyde (4.17 g, 30.66 mmol) and aniline (375 μL, 44.84 mmol) in ethanol (25 mL) was heated at reflux for 2 h. The solvent was evaporated, and the orange oil was treated with a chloroform/water mixture. The organic layer was dried over anhydrous Na_2SO_4 and the solvent evaporated. Yield: 6.33 g (30 mmol, 98%) of *N*-phenyl-3-methyl salicylaldimine. ^{1}H NMR ($DCCl_3$) δ: 8.63 (s, 1H, N═CH−), 7.44 (m, 2H, C4−H, C6−H), 7.28 (m, 5H, ph), 6.87 (t, 1H, C5−H), 2.34 (s, 3H, 3-CH_3). ^{13}C NMR ($DCCl_3$) δ: 162.84 (CH═N), 159.48, 148.54, 134.15, 129.99, 129.41 (×2), 126.81, 126.52, 121.17 (×2), 118.60, 118.44, (Ar), 15.73 (3-CH_3). To *N*-phenyl-3-methyl-salicylaldimine (6.33 g, 30 mmol) was added concentrated sulphuric acid (40 mL, 98 wt %, δ = 1.84 g/mL), and the mixture was stirred at 90 °C for 2 h. After cooling, the solution was added slowly to ice−water with vigorous stirring and a yellowish green solid precipitated. The mixture was reheated until all of the solid dissolved, and then it was allowed to cool. The yellow N-phenyl-3-methylsalicylaldimine-5-sulfonic acid was filtered off, washed with ice−water and ethanol, and dried under vacuum. Yield: 3.95 g (13.6 mmol, 45%). ^{1}H NMR (D_4-methanol/D_2O) δ: 9.22 (s, 1H, N═CH−), 8.26 (dd, 1H, C6−H), 8.14 (dd, 1H, C4−H), 7.79 (m, 5H, Ar), 2.55 (s, 3H, 3-CH_3). ^{13}C NMR (D_4-methanol/D_2O) δ: 162.05 (C2−OH), 158.73 (CH═N), 137.4, 135.96, 131.73, 131.38 (x2), 130.49, 130.37, 128.55, 124.17 (x2), 120.46 (Ar), 15.54 (3-CH_3). N-Phenyl-3-methylsalicylaldimine-5-sulfonic acid (3.95 g) in a saturated solution of Na_2CO_3 (23 mL) was boiled vigorously for 2 h. After cooling, glacial acetic acid was slowly added to pH 5 followed by ethanol (980 mL). The mixture was cooled to 0 °C, the pale yellow solid filtered off, washed with ethanol, and dried. Yield: 2.05 g (8.61 mmol, 63%) of sodium 3-methylsalicylaldehyde-5-sulfonate. ^{1}H NMR (D_2O) δ: 10.34 (s, 1H, O═CH−), 8.38 (dd, 1H, C6−H), 8.26 (dd, 1H, C4−H), 2.67 (s, 3H, 3-CH_3). ^{13}C NMR (D_2O) δ: 199.07 (CH═O), 162.18 (C2), 137.24, 135.98, 130.52, 128.69, 120.51 (Ar), 15.41 (3-CH_3). Significant IR bands (KBr, ν cm^{-1}): $\nu_{C=O}$ 1655, ν_{SO_3} 1112/1052.

Synthesis of Sodium Salt of 1,5-bis(3-methyl-5-sulphonatosalicylidenamino)pentan-3-ol (Na_2[3-Me-5-SO_3-salpentOH]·3H_2O). The ligand was prepared by Schiff-base condensation of sodium 3-methylsalicylaldehyde-5-sulfonate (1.90 g, 7.99 mmol) with 1,5-diaminopentan-3-ol[21] (3.99 mmol) in ethanol (50 mL), at reflux for 5 h. Na_2[3-Me-5-SO_3-salpentOH]·3H_2O was isolated as a pure yellow solid by precipitation from the reaction mixture at room temperature. Yield: 2.19 g (3.58 mmol, 90%). Anal. Calcd. for $C_{21}H_{24}N_2Na_2O_9S_2$·3$H_2O$: C 41.17, H 4.90; N 4.58%. Found: C 40.63; H 4.87; N 4.51%. ^{1}H NMR (D_2O) δ: 8.73 (s, 2H, N═CH−), 8.14 (d, 2H, C6−H), 7.92 (dd, 2H, C4−H), 4.16 (m, 4H, −C$\underline{H}_2$−N), 3.45 (m, 1H, H−C(OH)−), 2.50 (s, 6H, −CH_3), 2.29 (m, 4H, (HO)C−C$\underline{H}_2$−). ^{13}C NMR (D_2O) δ: 176.27 (Ar), 167.74 (CH═N), 133.15, 132.63, 127.03, 124.75, 121.93 (Ar), 66.49 ($R_2\underline{C}H$−OH), 48.16 (N−CH_2−), 36.04 (−$\underline{C}H_2$−CHOH−), 15.73 (3-CH_3). UV−vis λ_{max} nm (ε M^{-1} cm^{-1}) in H_2O: 222 (43000), 241 (25630), 277 (sh), 258 (sh), 333 (3950), 386 (3890). In Et_3N/Et_3NH^+ buffer, pH 10.75: 240 (50300), 259 (sh, 14700), 374 (9890). Significant IR bands (KBr, ν cm^{-1}): ν_{OH} 3426 (broad), $\nu_{C=N}$ 1646, ν_{SO_3} 1111/1041.

Synthesis of Na[Mn_2(3-Me-5-SO_3-salpentO)(μ-OAc)(μ-OMe)(H_2O)]·4H_2O (1). $Mn(OAc)_3$·2H_2O (1.36 g, 5.07 mmol) was added to a solution of Na_2[3-Me-5-SO_3-salpentOH]·3H_2O (1.53 g, 2.5 mmol) in methanol (50 mL). The mixture was stirred for 20 min, then filtered, and the resulting green solution was left to stir for 24 h. The green precipitate was collected by filtration, washed with cold methanol, and dried under vacuum. Yield 1.52 g (1.85 mmol, 74%). Anal. Calcd. for $Mn_2C_{24}H_{29}N_2O_{13}S_2Na$·4$H_2O$: C 35.04, H 4.53, Mn 13.36, N 3.41, Na 2.79%; found C 34.70, H 4.19, Mn 12.95, N 3.31, Na 2.80%. Significant IR bands (KBr, ν cm^{-1}): ν_{OH} 3440, ν_{CH} 2930, $\nu_{C=N}$ 1613, ν_{AcO} 1558/1432, ν_{SO_3} 1118/1042. UV−vis λ_{max} nm (ε M^{-1} cm^{-1}) in H_2O: 276 (29595), 360 (6450), 445 (sh, 2152), 592 (904). In Et_3N/Et_3NH^+ buffer, pH 10.75: 240 (70500), 260 (sh), 375 (19640). Molar conductivity = 74 Ω^{-1} cm^2 mol^{-1}. Single crystals of Na[Mn_2(3-Me-5-SO_3-salpentO)(μ-OMe)(μ-OAc)(MeOH)]·3MeOH (**1**(MeOH)) suitable for X-ray diffraction were obtained by crystallization of **1** from methanol upon standing in air for about one fortnight.

Physical Measurements. Electronic spectra were recorded on a JASCO V550 spectrophotometer with cell compartments thermostatted at 25 °C. IR spectra were recorded on a Perkin-Elmer Spectrum One FT-IR spectrophotometer. ESI-mass spectra were recorded on an API

365 MS mass spectrometer. The electrospray solutions were prepared from solutions of the complex or reaction mixtures and then diluted 100 times with methanol to reach a final $\approx 10^{-5}$ M concentration at a flow rate of 5 μL min^{-1}. EPR data were recorded using an Elexsys E 500 Bruker spectrometer, operating at a microwave frequency of approximately 9.5 GHz. All spectra were recorded using a microwave power of 0.5 mW (under nonsaturating conditions) with a modulation amplitude of 0.5 mT. Experiments were carried out at 110 K using a liquid nitrogen cryostat. ^{1}H and ^{13}C NMR spectra were recorded on a Bruker AC 300 NMR spectrometer at ambient probe temperature (ca. 25 °C). Paramagnetic spectra were recorded using the super WEFT sequence, with an acquisition time of 23 ms. Conductivity measurements were performed using a Horiba F-54 BW conductivity meter on 1.0 mM solutions of the complex in water. The electrochemical experiments were performed with a computer-controlled Princeton Applied Research potentiostat, model VERSASTAT II, with model 270/250 Research Electrochemistry Software. Studies were carried out under Ar in methanol solutions using 0.1 M Bu_4NPF_6 as a supporting electrolyte and $\approx 10^{-3}$ M of the complex. The working electrode was a Pt wire or a glassy carbon disk, and the reference electrode was Ag/AgCl with Pt as the auxiliary electrode. All potentials are referred to the Ag/AgCl electrode. Using the described conditions, the ferrocene/ferrocenium redox couple was observed at $E_{1/2}$ = 417 mV. Resonance Raman spectra were measured in backscattering geometry by using a confocal microscope (Olympus BX41) coupled to a single-stage spectrograph (Jobin Yvon XY 800) equipped with a liquid-nitrogen-cooled back-illuminated CCD detector and an 1800 L/mm grating. Elastic scattering was rejected with an edge filter (Semrock). The 514 nm line of a cw argon laser (Coherent Innova 70c) was focused into ca. 100 μL solution film in a rotating quartz cell using a 20× objective (20.5 mm wd, 0.35 N.A.). Spectra were acquired with laser powers of about 13 mW at the sample and were processed with homemade software for baseline correction and peak determination. Spectral positions were aligned toward standard Hg and Na lamps.

Volumetric Measurements. The stoichiometry of the reaction was measured by volumetric determination of the evolved O_2 from reaction mixtures in DMF, methanol, water, aqueous base, or buffer. A round-bottom flask with a stopcock equipped gas delivery side tube connected to a gas-measuring buret (precision of 0.1 mL) was used. A closed vessel containing a solution of catalyst was stirred at constant temperature on a water bath. Reactions in basic media were performed using aqueous NaOH or $Et_3N/Et_3NH\cdot ClO_4$ buffer. Previously thermostatted H_2O_2 ([H_2O_2]:[catalyst] ratio 150:1 or 175:1) was injected through a silicon stopper, and the evolved dioxygen was volumetrically measured. Blanc experiments performed in an Et_3N/Et_3NH^+ buffer (pH 10.5 to 11.1) without the catalyst showed that after 40 min only 5% of the initial H_2O_2 had disproportionated, while when the catalyst was present, all H_2O_2 decomposed in 1 min.

Kinetic Measurements. Oxygen evolution studies were carried out polarographically using a Clark-type oxygen electrode with an YSI oxygen-monitoring system (Model 5300, Yellow Springs Instruments Co., Inc.). The initial rate method was used to determine the rate constants (see ref 22 for further details). Each rate constant reported here represents the mean value of multiple determinations that fall within ±5%. Experiments were carried out at 25 °C.

X-ray Structure Determination. Crystallographic data for compound Na[Mn_2(3-Me-5-SO_3-salpentO)(μ-OMe)(μ-OAc)(MeOH)]·3MeOH were collected at 180(2) K on an Oxford-Diffraction GEMINI Diffractometer using a graphite-monochromated Mo-$K\alpha$ radiation (λ = 0.71073 Å) and equipped with an Oxford Cryosystems Cryostream cooler device. Unit cell determination, data collection, and reduction were carried out using the CrysAlis package.[23] The structure was solved by direct methods with SIR 92[24] and refined by full-matrix least-squares on Fo^2 with SHELXL-97,[25] using anisotropic displacement parameters for non-hydrogen atoms. Semiempirical absorption correction was applied with the aid of the program DIFABS.[26] The molecular plots were drawn using the CAMERON program,[27] with 50% probability displacement ellipsoids. Crystal data collection and refinement parameters are summarized in Table 1. In the crystal lattice, methanol molecules appear to be highly disordered, and it was difficult to model their positions and distribution reliably. Therefore, the SQUEEZE function of PLATON[28] was used to eliminate the contribution of the electron density in the solvent region from the intensity data, and the solvent free model was employed for the final refinement.

Table 1. Summary of Crystal Data for 1(MeOH)

empirical formula	$C_{27}H_{39}Mn_2N_2NaO_{15}S_2\cdot CH_4O$
M	860.65
temperature (K)	180
wavelength (Å)	0.71073
crystal system, space group	triclinic, $P\bar{1}$
a (Å)	11.3916(8)
b (Å)	12.3230(7)
c (Å)	15.8306(10)
α (deg)	100.284(5)
β (deg)	108.520(6)
γ (deg)	106.187(6)
V (Å^3)	1934.7(3)
Z	2
$\rho_{(calcd.)}$ (Mg/m^3)	1.477
μ_{Mo} (mm^{-1})	0.840
$F(000)$	892
crystal size (mm)	0.14 × 0.12 × 0.02
θ range (deg)	3.44 to 25.35
index ranges	$-13 \le h \le 13$, $-14 \le k \le 14$, $-19 \le k \le 19$
reflections collected/unique	29280/7057 [R(int) = 0.0875]
completeness to θ = 25.35	99.7%
refinement method	full-matrix least-squares on F^2
data/restraints/parameters	7057/25/477
goodness-of-fit on F^2	0.834
final R indices [$I > 2\sigma(I)$]	R_1 = 0.0463, wR_2 = 0.0885
R indices (all data)	R_1 = 0.1003, wR_2 = 0.0959
largest diff. peak and hole e (Å^{-3})	0.582 and −0.515

RESULTS AND DISCUSSION

Solid State Characterization of Complex 1. The N_2O_3 pentadentate symmetric ligand, 3-Me-5-SO_3-salpentOH, which provides an alkoxo oxygen for the endogenous bridging of two metal ions and two arms with N/O chelating donor sets, was reacted with 2 equiv of $Mn(OAc)_3\cdot 2H_2O$ in methanol to prepare a water-soluble diMn complex. In this reaction, acetate basicity facilitates deprotonation of the alcohol and phenol groups for coordination to the metal, to afford Na[Mn_2(3-Me-5-SO_3-salpentO)(μ-OAc)(μ-OMe)(H_2O)]·4H_2O (**1**). Although the disodium salt of the ligand was used, the analytical results show that the complex retains only one sodium ion per complex molecule in the solid state. The IR spectrum of complex **1** (Figure 1) exhibits strong imine and phenolate absorptions at 1613 and 1545 cm^{-1} that are shifted by ≈30 cm^{-1} from those in the free ligand due to the coordination of the metal to these groups. The two strong bands at 1118 and 1042 cm^{-1} are

dx.doi.org/10.1021/ic2011452 |Inorg. Chem. 2011, 50, 8973–8983

attributable to the antisymmetric and symmetric stretching modes of the $-SO_3^-$ groups, and absorption peaks at 1558 and 1432 cm^{-1} identify the antisymmetric and symmetric stretching vibrations of the *syn,syn*-1,3-bridging acetate.[29] Comparison of the FT-IR spectrum of **1** with those of other $diMn^{III}$ complexes of the X-salpentOH family[30] evidence the fingerprint pattern of the Schiff-base ligand and $\mu_{1,3}$-carboxylato coordinated to the Mn ions.

Crystal Structure of Na[Mn_2(3-Me-5-SO_3-salpentO)(μ-OAc)(μ-OMe)(MeOH)]·3MeOH (1(MeOH)). Single crystals of Na[Mn_2(3-Me-5-SO_3-salpentO)(μ-OAc)(μ-OMe)(MeOH)]·3MeOH (**1**(MeOH)) suitable for X-ray diffraction studies were obtained by slow evaporation of a methanol solution of **1**. The asymmetric unit of **1**(MeOH) contains one diMn complex anion, one sodium cation, and solvate methanol molecules. The molecular structure of complex **1**(MeOH) is illustrated in Figure 2. In each complex anion, 3-Me-5-SO_3-salpentO^{5-} acts as a pentadentate ligand through the N_2O_3 donor set. The two Mn atoms are six-coordinated and triply bridged by the central alkoxo of 3-Me-5-SO_3-salpentO^{5-} and exogenous *syn,syn*-acetato and methoxo ligands. The phenolato-*O*, imino-*N*, and alkoxo-*O* atoms of the ligand and the methoxo-*O* donor atom form a meridional geometry around each Mn. One of the axial positions of each Mn atom is occupied by an acetato-*O* atom, and the sixth coordination position of Mn(2) is occupied by one oxygen atom from an exogenous methanol molecule and that of Mn(1) by one oxygen atom of the sulphonato group of an adjacent complex molecule. The Mn−N/O bond lengths listed in Table 2 are typical of the Mn^{III} oxidation state.[31−34] The coordination polyhedra of the Mn centers may be described as elongated octahedra, with the axial Mn−O bond distances (av. 2.238(3) Å) distinctly longer than the equatorial Mn−N/O ones (av. 1.925(3) Å), a clear signature of the Jahn−Teller distorted coordination sphere of Mn^{III} ions. The deviation from an ideal octahedral geometry is also revealed by the range of angles observed around each metal center (from 78.58(12)° to

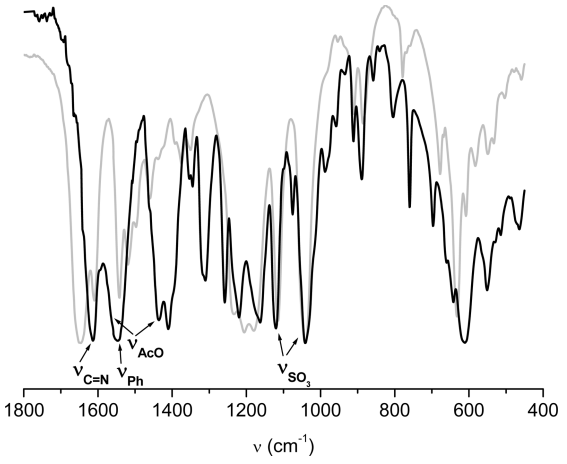

Figure 1. FT-IR spectra of complex **1** (black) and Na_2[3-Me-5-SO_3-salpentOH] (gray).

Table 2. Selected Bond Lengths and Angles for Na[Mn_2(3-Me-5-SO_3-salpentO)(μ-OMe)(μ-OAc)(MeOH)]·3MeOH (1(MeOH))

bond lengths (Å)			
Mn(1)−O(1)	1.842(3)	Mn(2)−O(2)	1.925(3)
Mn(1)−O(2)	1.910(3)	Mn(2)−O(3)	1.849(3)
Mn(1)−O(4)	1.933(3)	Mn(2)−O(4)	1.933(3)
Mn(1)−O(5)	2.238(3)	Mn(2)−O(6)	2.220(3)
Mn(1)−O(7)	2.262(3)	Mn(2)−O(12)	2.232(4)
Mn(1)−N(2)	2.005(4)	Mn(2)−N(1)	1.999(4)
angles (deg)			
O(1)−Mn(1)−O(2)	170.48(13)	O(3)−Mn(2)−O(2)	171.79(12)
O(1)−Mn(1)−O(4)	91.84(12)	O(3)−Mn(2)−O(4)	93.24(13)
O(2)−Mn(1)−O(4)	78.94(12)	O(2)−Mn(2)−O(4)	78.58(12)
O(1)−Mn(1)−N(2)	92.67(13)	O(3)−Mn(2)−N(1)	91.68(14)
O(2)−Mn(1)−N(2)	96.55(13)	O(2)−Mn(2)−N(1)	96.52(14)
O(4)−Mn(1)−N(2)	175.48(13)	O(4)−Mn(2)−N(1)	174.47(15)
O(1)−Mn(1)−O(5)	90.06(13)	O(3)−Mn(2)−O(6)	90.17(13)
O(2)−Mn(1)−O(5)	88.26(13)	O(2)−Mn(2)−O(6)	89.19(13)
O(4)−Mn(1)−O(5)	94.01(13)	O(4)−Mn(2)−O(6)	90.96(12)
N(2)−Mn(1)−O(5)	85.78(14)	N(1)−Mn(2)−O(6)	91.53(15)
O(1)−Mn(1)−O(7)	92.67(12)	O(3)−Mn(2)−O(12)	89.74(14)
O(2)−Mn(1)−O(7)	90.27(12)	O(2)−Mn(2)−O(12)	91.44(14)
O(4)−Mn(1)−O(7)	93.45(13)	O(4)−Mn(2)−O(12)	92.86(13)
N(2)−Mn(1)−O(7)	86.55(14)	N(1)−Mn(2)−O(12)	84.66(15)
O(5)−Mn(1)−O(7)	171.97(12)	O(6)−Mn(2)−O(12)	176.18(12)
Mn(1)−O(2)−Mn(2)	99.76(13)	Mn(1)−O(4)−Mn(2)	98.68(13)

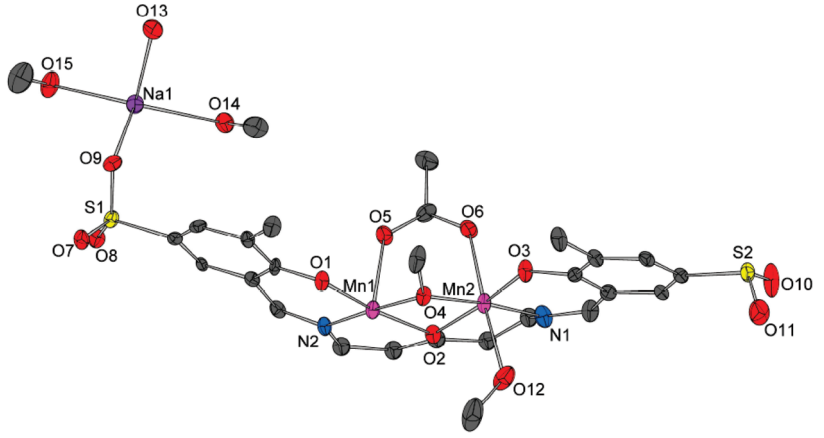

Figure 2. Asymmetric unit of **1**(MeOH) with atom numbering.

dx.doi.org/10.1021/ic2011452 |*Inorg. Chem.* 2011, 50, 8973–8983

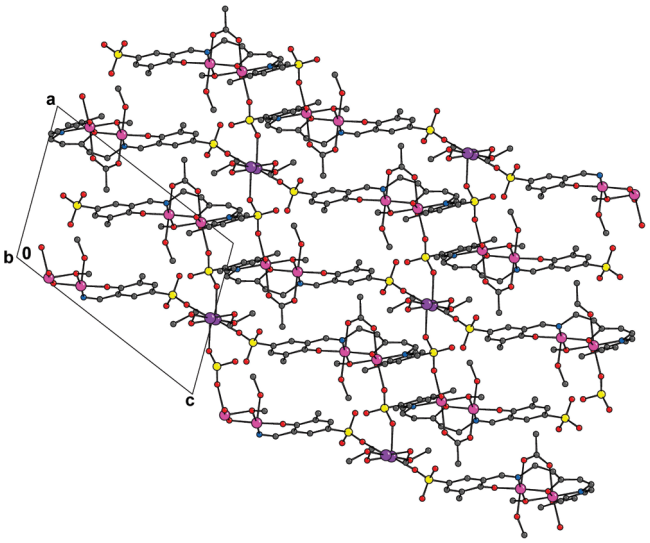

Figure 3. Packing diagram of **1**(MeOH) viewed along the crystallographic *b* axis.

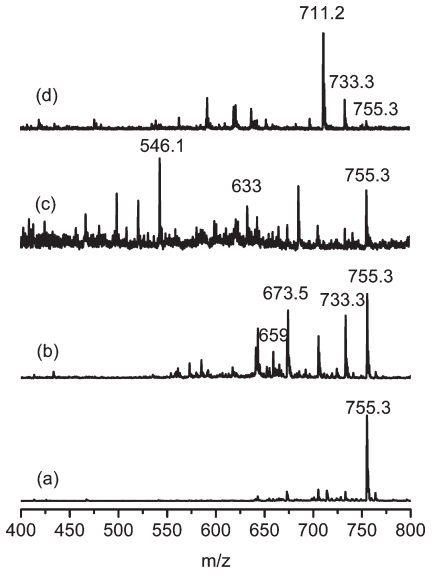

Figure 4. ESI-mass spectra of (a) **1** in methanol and (b) **1** in H_2O; (c) a reaction mixture of **1** + 5 equiv NaOH + 100 equiv H_2O_2, in H_2O; (d) **1** + 150 equiv H_2O_2, in Et_3N/Et_3NH^+ buffer, after reaction.

96.55(13)°). The Mn···Mn separation (2.933(1) Å) and the Mn−O−Mn angles (98.68(13)−99.76(13)°) defining the core of the asymmetric unit are typical of triply bridged bis(μ-alkoxo)(μ-carboxylato) $diMn^{III}$ complexes of polydentate ligands derived from 1,5-diaminopentan-3-ol[30,35] and smaller than those of Mn^{III}_2 complexes of polydentate ligands derived from 1,3-diaminopropan-2-ol (≈ 3.2 Å), which possess a Jahn−Teller elongation axis oriented along the bridging core.[32,34,36−38]

Figure 3 displays the packing structure parallel *ac* plane of compound **1**(MeOH). In the crystal structure, each dinuclear entity is connected to an adjacent diMn anion through coordination of Mn(1) and O(7) of the sulphonato group of the basic dinuclear unit to the respective O(7) and Mn(1) of a neighbor complex anion. Additionally, the Na cations link each dimanganese unit to its symmetrically related congener through

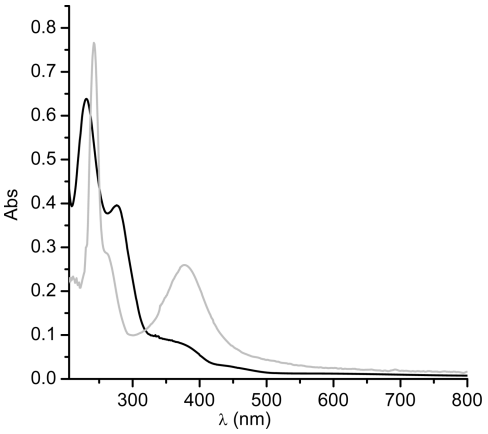

Figure 5. Electronic spectra of 1.3×10^{-5} M **1** in H_2O (black) and buffer of pH 10.75 (gray); l = 1 cm.

Na−O-sulphonato bonds (see Figure S1 in the Supporting Information), and in turn, each Na^+ is attached to a near Na^+ through methanol bridges, thus reinforcing an overall 3-D structure.

Solution Studies. *ESI-Mass Spectrometry (ESI-MS).* ESI-mass spectra of complex **1** confirmed its chemical composition as well as retention of nuclearity in solution. The positive mode mass spectrum of **1** in methanol (Figure 4a) is dominated by the peak at m/z = 755.3 (100%) and originates from the monocation $Na_2[Mn^{III}_2L(OAc)(OMe)]^+$. The positive mode ESI-mass spectrum of **1** in water (Figure 4b) exhibits, besides the parent peak at m/z = 755.3 (100%), three other major peaks at m/z = 733.3 (84%, $HNa[Mn^{III}_2L(OAc)(OMe)]^+$) where one Na^+ is replaced by H^+, m/z = 673.5 (88%, $Na[Mn^{III}_2L(OMe)]^+$) corresponding to the loss of acetate, and m/z = 659.0 (41%, $Na[Mn^{III}_2L(OH)]^+$) where the methoxo bridging ligand is substituted by a hydroxo originated from the solvent in the latter species. Additional peaks at m/z 764.3 (11%), 705.3 (60%), and 643.2 (69%), corresponding to the $Na_3[Mn^{II,III}_2L(OAc)(OH)]^+$ mixed valence and $Na_3[Mn^{II}_2L(OH)]^+$ and $NaH[Mn^{II}_2L]^+$ cations also appear in the ESI-mass spectra of the complex. These species are most likely to be generated within the spectrometer. Upon the addition of NaOH to an aqueous solution of **1**, $Na_2[Mn^{III}_2L(OAc)(OMe)]^+$ (m/z 755.3) is observed together with other monocations generated during the electrospray experiments, with the main corresponding to $H[Mn^{IV}_2L(OMe)(OH)_2]^+$ (m/z 685.5), $H_3[Mn^{II,III}_2L(OH)_2]^+$ (m/z 656.3), and $Na_3[Mn^{III}L]^+$ (m/z = 633.0). In the Et_3N/Et_3NH^+ buffer, even when the ESI-mass spectra are dominated by the peak of the buffer (m/z = 303.5, $[(Et_3NH)_2(ClO_4)]^+$, 100%), monocations $H_2[Mn^{III}_2L(OAc)(OMe)]^+$ (m/z = 711.2) and $NaH[Mn_2L(OAc)(OMe)]^+$ (m/z = 733.3) could be well identified as main species.

Electronic Spectroscopy. The electronic spectrum of **1** in H_2O (Figure 5, black) shows an intense absorption at 276 nm which can be attributed to intraligand $\pi-\pi^*$ transitions. Absorptions in the 350−500 nm range correspond to ligand-centered transitions overlapping with L→M charge-transfer transitions from $p\pi$ orbitals of the phenoxo oxygen to the partially filled $d\pi$ orbitals of the Mn^{III} ion, as also observed for other $diMn^{III}$ complexes with phenoxo ligands.[39−42] Absorption at 592 nm (ε = 904 M^{-1} cm^{-1}) can be assigned to a d-d transition in agreement with reported values for related $diMn^{III}$ complexes.[35,39−41]

dx.doi.org/10.1021/ic2011452 |*Inorg. Chem.* 2011, 50, 8973–8983

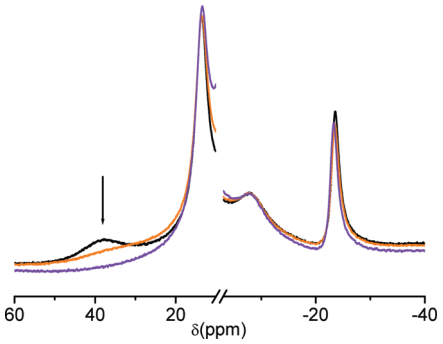

Figure 6. ^{1}H NMR spectra of **1** (20 mM), before (black) and after the addition of 1.25 (orange) and 5.0 equiv (purple) of NaOH, in D_4-methanol.

UV−vis spectra of basic solutions of complex **1**, in either a NaOH, Et_3N, or Et_3N/Et_3NH^+ buffer, show an intense absorption at 375 nm due to intraligand transitions of the sulphonato ligand superimposed to phenolate to Mn^{III} CT transitions (Figure 5, gray). The intensity of this absorption is around twice that of the free ligand, and the results are useful to monitor the integrity of the catalyst during H_2O_2 disproportionation. In these basic solutions, no discernible bands corresponding to d-d transitions have been resolved in the lower energy visible region.

^{1}H NMR Spectroscopy. ^{1}H NMR spectra of mono- and dinuclear Mn^{III}-salycilidenamino complexes display a set of upfield resonances corresponding to protons of the phenolato ring that has proven to be particularly valuable in the characterization of the species in solution.[43a] The paramagnetic ^{1}H NMR spectrum of **1** in D_4-methanol contains a characteristic acetate peak and distinctive ligand resonances that reveal a pattern typical of a highly symmetrical environment for the Schiff base ligand (Figure 6) and confirms that this complex retains its dinuclear structure in solution. The spectrum shows two broad upfield resonances at −23.54 and −7.75 ppm, assigned to the H4 and H6 protons of the two magnetically equivalent terminal phenolate rings, in accordance with previous studies.[43] The intense resonance that appears at 13.51 ppm corresponds to the methyl substituent in the aromatic ring. This peak shows the broadened features of a paramagnetic signal, and the assignment is further confirmed by comparison with the corresponding spectrum of $[Mn_2(\mu\text{-OAc})(\mu\text{-OMe})(3\text{-Me-salpentO})]$.[30b] The broad resonance at 38 ppm can be assigned to the methyl group of the bridging acetate of **1** on the basis of comparison with the spectra of other $Mn^{III}{}_2(\mu\text{-OAc})$ complexes previously studied.[43b,c]

The effect of the addition of base on the ^{1}H NMR spectrum of **1** in D_4-methanol was examined. Spectra taken after the addition of increasing amounts of NaOH (from 1 to 5 equiv) showed that the proton resonances from the Schiff base ligand remain unchanged, but the intensity of the bridging acetate protons decreased and the peak disappeared when 5 equiv of base were added (Figure 6). The same decrease of the resonance of the bridging acetato protons was observed upon the addition of 5 equiv of Et_3N. The unchanging paramagnetic shift of the ligand protons indicates that the magnetic coupling between Mn ions is the same as in starting **1**. Besides, ESI-MS results described above showed that in a basic medium the complex retains acetate. Therefore, the disappearance of the broad resonance corresponding to the acetate protons together with the unchanged chemical shift of the aromatic protons can be interpreted in terms

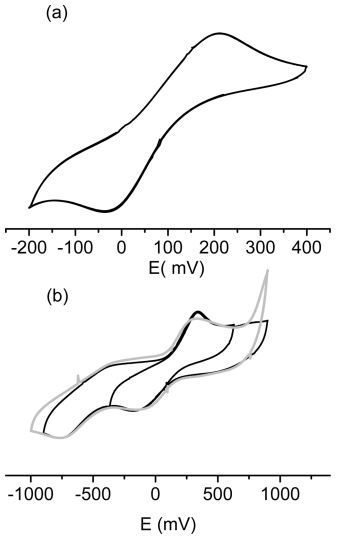

Figure 7. Cyclic voltammogram of (a) **1** in methanol: scan rate = 100 mV/s, working electrode = Pt wire; (b) **1** in methanol, before (black) and after the addition of Et_3N (gray): scan rate = 300 mV/s, working electrode = glassy carbon. Conc. = 1 mM. Supporting electrolyte = Bu_4NPF_6. Reference electrode = AgCl/Ag.

of the conversion of bridging acetate into a monodentate terminal ligand, chemical shift of monodentate acetate being within the diamagnetic region of the spectrum, which might accommodate the coordination of an additional terminal base ligand.[44a] ^{1}H NMR spectra obtained in a basic medium also exclude the formation of an oxo-bridged $Mn^{III}{}_2$, which should provide a better exchange pathway between Mn ions affording a spectrum with paramagnetic shifts different from those of the starting compound.[43a,44]

Electrochemical Studies. The electrochemical properties of complex **1** were investigated by cyclic voltammetry in methanol solutions containing 0.1 M Bu_4NPF_6, using a Ag/AgCl reference electrode. The complex exhibits one quasi-reversible wave at $E_{1/2}$ 95 mV (ΔE_p = 200 mV, Figure 7a) that can be attributed to the $Mn^{III}{}_2/Mn^{III}Mn^{II}$ redox couple, as confirmed by linear and square-wave voltammetry ($w_{1/2}$ = 120 mV) experiments. An additional nonreversible reduction peak was observed at −570 mV in the cathodic scan (Figure 7b, black), attributable to the $Mn^{III}Mn^{II}/Mn^{II}{}_2$ couple, as suggested for previously reported complexes with a similar ligand environment.[30,32] Upon addition of Et_3N to the MeOH solution of **1**, no changes were observed in the cyclic voltammogram, a result that excludes the conversion of the starting complex into the μ-oxo-Mn_2 complex, the signature of which is significantly different,[41,45] and is consistent with the ^{1}H NMR results. An irreversible peak at $E_p \approx$ 850 mV was also observed in the oxidative scan, but it was already present in the voltammogram of the Et_3N/MeOH mixture.

CAT Activity Studies. *Sensitivity of the Catalase Activity of **1** to the Reaction Medium.* The ability of complex **1** to catalyze H_2O_2 disproportionation was tested in DMF, methanol, and water. Addition of H_2O_2 to a solution of the catalyst causes an immediate vigorous evolution of dioxygen coupled to color changes: from green to orange in DMF and from green to pale yellow in methanol and water. The relative CAT activity of **1** in these solvents was determined by the volumetric measurement of evolved O_2. As shown in Figure 8, complex **1** dismutates 150 equiv of H_2O_2 within 11 min in DMF, whereas it requires more

dx.doi.org/10.1021/ic2011452 |*Inorg. Chem.* 2011, 50, 8973–8983

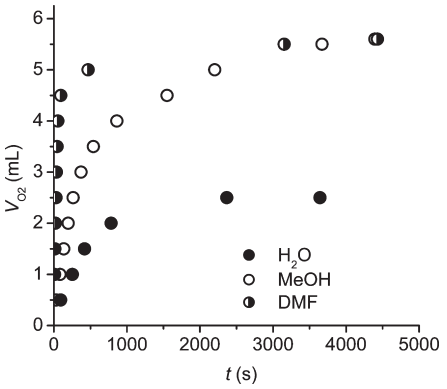

Figure 8. Time-dependence of O_2 evolution upon reaction of **1** with 150 equiv of H_2O_2 in different solvents. [**1**] = 1×10^{-3} M; T = 25 °C.

than 1 h to dismutate the same H_2O_2 amount in methanol. In water, H_2O_2 disproportionation is still slower, and the catalyst inactivates after the disproportionation of 70 equiv of H_2O_2. Successive additions of 150 equiv of H_2O_2 to the catalyst solution showed that complex **1** is able to disproportionate more than 1500 equiv of H_2O_2 in DMF without significant decomposition, but in methanol, it inactivates after 200 turnovers. It is likely that the bridging ligands of the complex serve as internal bases facilitating deprotonation of the peroxide coupled to the redox reaction. Therefore, in the protic solvents, protonation of these bridges may result in the inactivation of the catalyst and metal dissociation during the reaction.

Given the particular interest of evaluating the CAT activity in aqueous solution, and with the intention to avoid inactivation of the catalyst in the protic solvent, H_2O_2 disproportionation by complex **1** was measured in aqueous NaOH (pH 12.4). Successive additions of excess H_2O_2 to the catalyst in aqueous NaOH solution yielded the stoichiometric amount of O_2, but the initial rate of H_2O_2 dismutation gradually decreased after each new addition (Figure 9a). UV−vis spectra taken at different reaction times showed an intensity decrease of the absorption at 375 nm, indicating a partial loss of catalyst after successive additions of H_2O_2. This was confirmed by ESI-mass spectra taken at the end of the reaction of **1** with excess H_2O_2 in aqueous NaOH, that showed an intensity decrease of the peak corresponding to $Na_2[Mn^{III}{}_2(OAc)(OMe)L]^+$ (m/z 755.3) and an increase of peaks corresponding to $Na_3[Mn^{III}L]^+$ (m/z 633.0) and $H_2[L(MeOH)]^+$ (m/z 546.1) relative to that of the dinuclear complex (Figure 4c). EPR monitoring of reaction mixtures in aqueous NaOH provided complementary information on the inactive form of the catalyst. EPR spectra of a 1:5:150 **1**:NaOH:H_2O_2 reaction mixture showed, in the region of g ≈ 2, a 6-line signal (hyperfine splitting of ≈90 G) characteristic of an $Mn^{2+}{}_{aq}$ ion (Figure 9c). This EPR signal grew-in and persisted at the end of the reaction, indicating accumulation of an inactive Mn^{II} species is responsible for the loss of catalytic activity. Therefore, as NaOH was consumed, the pH of the reaction mixture decreased (from 12.4 to 8.2 after 12 additions of 150 equiv of H_2O_2), and protonation of the catalyst began to compete with CAT activity, lowering the efficiency to disproportionate H_2O_2. This problem was solved by performing the reaction in a buffered basic solution. Different buffers were tested in order to find the optimal pH for the highest catalytic efficiency. It was found that the pH must be controlled to values ≥ 8.5 for the catalyst to retain its efficiency after successive additions of H_2O_2. Excellent results

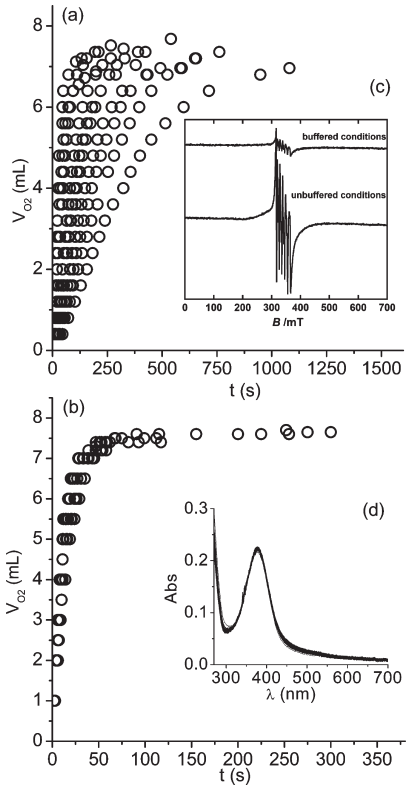

Figure 9. Time-dependence of O_2 evolution after succesive additions of 63 μL of 10.05 M H_2O_2 (175 equiv) to an (a) aqueous solution of **1** (1.2×10^{-3} M) + 5 equiv NaOH; and (b) **1** in a buffer at pH 10.75. (c) EPR spectra taken at the end of H_2O_2 disproportionation in NaOH and a buffer; ν = 9.5 GHz, T = 100 K, and microwave power = 0.5 mW. (d) Electronic spectra registered after successive additions of H_2O_2 to the solution of **1** (1.1×10^{-5} M) in a buffer at pH 10.75 and T = 298 K.

were obtained with an aqueous Et_3N/Et_3NH^+ buffer. More than 2500 turnovers were measured for complex **1** in the aqueous Et_3N/Et_3NH^+ buffer of pH 10.75, with only a slight decrease of activity (Figure 9b) and without significant decomposition, as shown by the spectrophotometric monitoring of the buffered reaction (Figure 9d). The observation of peaks corresponding to $H_2[Mn^{III}{}_2L(OAc)(OMe)]^+$ and $HNa[Mn^{III}{}_2L(OAc)(OMe)]^+$ at m/z = 711.2 and 733.3, respectively, in the ESI-mass spectra registered during and at the end of the reaction in the Et_3N/Et_3NH^+ buffer (Figure 4d) provide a clear indication that the $Mn^{III}{}_2$ complex persists during the catalytic cycle. The EPR spectra of complex **1** recorded in buffered solutions at various time-intervals following the addition of 150 equiv of H_2O_2 were essentially EPR silent, except for a very small six-line signal at g ≈ 2 with hyperfine splitting of ≈90 G (Figure 9c). Therefore, the $Mn^{2+}{}_{aq}$ species is only a minor one when the reaction is performed in a buffered solution (the intensity of the EPR signal of a 150:1 H_2O_2/catalyst mixture in an Et_3N/Et_3NH^+ buffer was less than 10% of that for the same reaction performed in aqueous NaOH). The absence of the EPR signal during the reaction course, except for the minor inactive Mn^{II} species, suggests that the $Mn^{III}{}_2$ form of the catalyst is the dominant species in solution since no EPR signal is expected for the catalyst in this oxidation state.

Raman and UV−vis Studies of the CAT-Reaction in DMF. In order to obtain additional information on the diMn species

dx.doi.org/10.1021/ic2011452 |*Inorg. Chem.* 2011, 50, 8973–8983

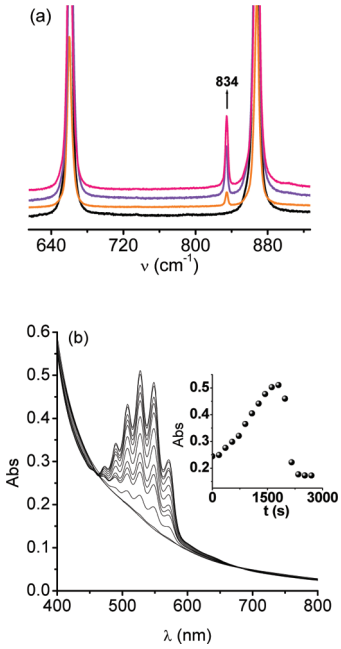

Figure 10. (a) RR spectra of a DMF solution of **1** (black) and a mixture of **1** + 150 equiv H_2O_2 + 5 equiv Bu_4NOH at 6 (orange), 9 (purple), and 16 min (pink) after mixing. 514 nm excitation; [**1**] = 0.6 mM. (b) Time-evolution of the multiplet at 528 nm in the electronic spectra of a DMF reaction mixture under conditions of the RR experiments. The inset: Abs vs time curve at 528 nm.

involved in the H_2O_2 disproportionation in basic medium, a mixture of **1** + 150 equiv H_2O_2 + 5 equiv Bu_4NOH in DMF was monitored by resonance Raman (RR) spectroscopy. DMF was used because neither water nor MeOH showed enhanced lines in the RR spectra. The RR spectra were obtained with 514 nm excitation and recorded at different times during the reaction (Figure 10a). Addition of H_2O_2 to the basic DMF solution of **1** changed the color of the solution from orange to pink during O_2 evolution and led to the appearance of a strongly enhanced Raman peak at 834 cm^{-1}. This peak grew up during the progress of the reaction and disappeared when the reaction was over. The signal reappeared with a second addition of 150 equiv of H_2O_2 to the DMF basic solution of the catalyst. The observed frequency at 834 cm^{-1} is consistent with the double-bond character between the Mn ion and an oxygen atom and is in the range expected for the Mn^{IV}=O stretching vibration in organic solvents.[46] In the present case, the Mn^{IV}=O frequency is higher than that of Mn^{IV}-oxo porphyrin complexes, in accordance with previous observation that the Mn-oxo complexes bearing non-porphyrinic ligands exhibit a Mn−O stretching band at higher frequency,[47] a fact that was attributed to the porphyrin π delocalization that weakens oxo → d_π donation.

The spectrophotometric monitoring of the reaction under the same conditions used in the RR experiments showed that, as the reaction progressed, a multiplet appeared centered at 528 nm with the line separation of ca. 20 nm (Figure 10b), reached a maximum, and then decreased (Abs^{528} vs time profile is shown in the inset of Figure 10b). After a new addition of 150 equiv of H_2O_2 to the catalyst, the multiplet reappeared during O_2 evolution and disappeared when the O_2 evolution had ceased. This multiplet, which parallels the kinetic profile of the peak at 834 cm^{-1} in the RR spectra, can be assigned to an oxo-to-manganese

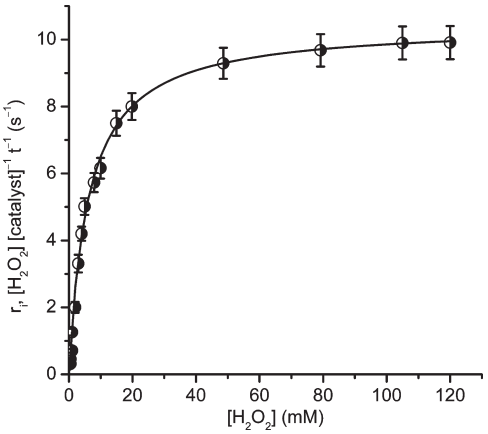

Figure 11. Effect of the H_2O_2 concentration on the initial rate of H_2O_2 disproportionation at 25 °C in an aqueous Et_3N buffer pH 10.6.

LMCT coupled to the $\nu_{Mn=O}$ vibration.[48] The fact that after successive additions of H_2O_2 the activity of **1** remains essentially constant and the recovery of the catalyst at the end of the reaction support that the Mn=O species observed in RR and electronic spectra still bears the ligand.

In order to verify if the strong enhanced Raman peak was also observed during the reaction of other diMn^{III} complexes of the X-salpentOH family in DMF solution of Bu_4NOH, two other complexes, [Mn_2(5-NO_2-salpentO)(μ-OMe)(μ-OAc)]Br and [Mn_2(naphpentO)(μ-OMe)(μ-OAc)]ClO_4, were studied by RR spectroscopy. H_2O_2 disproportionation catalyzed by these two complexes in Bu_4NOH/DMF also exhibit the multiplet centered at 528 nm in the visible spectra. The enhanced Raman peak is also observed at 834 cm^{-1} during the reaction of the two complexes with H_2O_2 (see Figure S2 in the Supporting Information), indicating that its frequency is independent of the substituent in the aromatic ring of the ligand. Therefore, UV−vis and RR spectroscopy agree that Mn^{IV}-oxo species are involved in the catalytic disproportionation of H_2O_2 by complexes of the X-salpentOH series in DMF, although the exact role of this solvent in delaying the reduction of the oxidized form of the catalyst to the diMn^{III} species is not yet clear.

Even when there is no direct evidence to discern if the catalyst shuttles between $Mn^{III}{}_2/Mn^{II}{}_2$ or $Mn^{III}{}_2/Mn^{IV}{}_2$ oxidations states during catalysis in an aqueous basic medium, spectroscopic observation of the oxo-Mn^{IV} species in basic DMF suggests that catalytic disproportionation of H_2O_2 by **1** involves $Mn^{III}{}_2/Mn^{IV}{}_2$ oxidation levels. In a basic aqueous solution, oxo-Mn^{IV} reduction should occur in a fast step of the catalytic cycle (fast oxidative half-reaction). Thus, the $Mn^{III}{}_2$ species should be the catalytic form that participates in the slow reductive half-reaction (turnover-limiting step) and the major form of the catalyst during catalysis, such as that observed.

Kinetics. The initial rate of H_2O_2 disproportionation by complex **1** was measured as a function of the complex and substrate concentrations, in the Et_3N/Et_3NH^+ buffer of pH 10.6, at 25 °C. At constant $[H_2O_2]_0$, the initial rate of H_2O_2 disproportionation varies linearly with the [catalyst], meaning that the reaction is first-order on the catalyst. The first order dependence of the reaction rate on the catalyst and the lack of time-lag at the onset of the reaction suggest that the starting complex is responsible for the rapid disproportionation of H_2O_2. At constant [catalyst], the initial rate of H_2O_2 dismutation

Table 3. k_{cat} and K_M Values for 1 and Other Dimanaganese CAT Models

	catalyst[a,b]	k_{cat} (s^{-1})	K_M (mM)	k_{cat}/K_M (s^{-1} M^{-1})	solvent, T (°C)	ref
1	**1**	10.5(2)	6.6(4)	$16(1) \times 10^2$	H_2O (pH 10.6), 25	this work
2	$[Mn^{IV}_2(salpn)(\mu\text{-}O)]_2$	250	250	1000	Cl_2CH_2/CH_3CN, 25	44b,44d
3	$[Mn(X\text{-}salpnO)]_2$	4.2−21.9	10−102	305−990	CH_3CN, 25	49
4	$[Mn_2(\mu\text{-}OAc)(\mu\text{-}OH_2)$ (benzimpnO)$]^{2+}$ + 5 equiv OH^-	2.1	3	700	MeOH:H_2O (89:11), 25	50
5	$[Mn_2(\mu\text{-}OMe)(\mu\text{-}OAc)(X\text{-}salpentO)S_2]^+$	0.75−7.9	16−66	25−102	DMF, 25	22,30
6	$[Mn_2(\mu\text{-}OMe)(\mu\text{-}OAc)(X\text{-}salpentO)S_2]^+$	0.48−6.2	13−201	8−70	MeOH, 25	22,30
7	$[Mn_2(\mu\text{-}OMe)(OAc)(X\text{-}hppentO)]^+$	1.31−2.8	88−170	15−100	DMF, 10	35
8	$[Mn_2(\mu\text{-}OAc)_2(X\text{-}hppnO)]^+$	3.4−23	150−600	22−38	DMF, 25	9
9	$Mn_2(\mu\text{-}OAc)_2(bphpmp)]^+$	2.48	83[c]	30	NR, 25	40
10	$[Mn(bpia)(\mu\text{-}OAc)]_2^{2+}$	0.237	45	5.2	DMF, 25	51,52
11	$[Mn_2(mesalim)_2(MeOH)]^{2+}$ + 5 equiv OH^-	0.038	21	1.8	EtOH, 25	52,53

[a] Ligands: H_2salpn = 1,3-bis(salicylideneiminato)propane, salpnOH = 1,3-bis(salicylideneamino)propan-2-ol, benzimpn = *N*,*N*,*N*′,*N*′-tetrakis(2-methylenebenzimidazolyl)-1,3-diaminopropan-2-ol, hppentOH = 1,5-bis[(2-hydroxybenzyl)(2-pyridylmethyl)amino]pentan-3-ol, hppnOH = 1,3-bis[(2-hydroxybenzyl)(2-pyridylmethyl)amino]propan-2-ol, bphpmp = 2-[bis(2-pyridylmethyl)aminomethyl]-6-{[(2-hydroxybenzyl)(2-pyridylmethyl))-amino]methyl}-4-methylphenol, bpia = bis(picolyl)(*N*-methylimidazol-2-yl)amine, mesalim = methyl salicylimidate, X = aromatic substituent, and S = solvent or labile anion. [b] For ligand formulas, see Scheme S1 in the Supporting Information. [c] mmol. NR = not reported.

exhibits saturation kinetics with $[H_2O_2]_0$ (Figure 11), and the experimental data could be fitted to the Michaelis−Menten equation, from which the catalytic turnover number k_{cat} = 10.5 ± 0.2 s^{-1} and the Michaelis constant K_M = 6.6 ± 0.4 mM were determined. On the basis of the k_{cat}/K_M criterion, complex **1**, with $k_{cat}/K_M = 16(1) \times 10^2$ s^{-1} M^{-1}, is the most efficient catalyst for H_2O_2 disproportionation reported to date. By examining Table 3, it can be seen that, independently of the solvent, complexes with $Mn_2(\mu\text{-}OR)_i(\mu\text{-}OAc)_j^{3+(or\ 4+)}$ or $Mn_2(\mu\text{-}OAc)_2(\mu\text{-}OPh)^{2+}$ cores disproportionate H_2O_2 with a k_{cat} in the range of 2−23 s^{-1} (entries 1, 3−9, Table 2),[9,22,30,35,40,49,50] but these values are significantly higher than those found for complexes possessing $Mn_2(\mu\text{-}OAc)_2^{2+}$ or $Mn_2(\mu\text{-}OPh)_2^{2+(or\ 4+)}$ cores (0.02−0.2 s^{-1})[51−53] (entries 10 − 11). $[Mn^{IV}(salpn)(\mu\text{-}O)]_2$ (entry 2, Table 3) disproportionates H_2O_2 with a rate higher than any of the other studied compounds, probably because the two endogenous μ-oxo-ligands are better internal bases to assist deprotonation of H_2O_2 coupled to its two-electron oxidation;[44b,d] however, this complex has a very poor affinity for the substrate (high K_M value), a fact probably resulting from the lack of labile positions to react with the substrate, which forces initial peroxide binding to occur through ligand exchange. The improved efficiency of **1** relative to other alkoxo- or phenoxo-bridged complexes results from its high affinity for the substrate (low value of K_M). At pH 10.6, H_2O_2 coexists with HO_2^-; thus, the higher affinity of HO_2^- vs H_2O_2 for binding **1** may also contribute to the observed K_M value. In fact, the K_M value found for **1** is lower than those of any other complex of the salpentOH family evaluated in DMF and methanol,[22,30] evidencing that it is the basic aqueous medium that favors peroxide binding to these catalysts. This is consistent with the enhancement of the affinity found for $[Mn_2(\mu\text{-}OAc)(\mu\text{-}OH_2)(benzimpnO)]^{2+}$ upon addition of 5 equiv OH^- in 89:11 MeOH:H_2O mixtures, which varies from K_M = 35 mM in methanol to K_M = 3 mM in the basic medium.[50] In line with this, the K_M value of **1** in the aqueous base is much lower than K_M = 189 mM found for $[Mn_2(\mu\text{-}OAc)(\mu\text{-}OMe)(3\text{-}Me\text{-}salpentO)]^+$ in methanol (α_{MeOH} = 0.93[54]).[30b] These results evidence the significant effect of protons on lowering the H_2O_2 affinity of these complexes and the efficiency of the buffer to offset this effect.

CONCLUSIONS

3-Me-5-SO_3-salpentOH affords complex **1**, a water-soluble diMn complex highly efficient to disproportionate H_2O_2 in an aqueous solution of pH ≥ 8.5. This complex possesses a triply bridged bis(μ-alkoxo)($\mu_{1,3}$-carboxylato) $diMn^{III}$ core that mimics the geometrical motif and coordination environment of the Mn^{III}_2 form of Mn catalases.[5] Spectroscopic monitoring of catalyzed H_2O_2 disproportionation in an aqueous buffer solution reveals that the major active form of the catalyst occurs in the Mn^{III}_2 oxidation state during cycling and that the starting complex retains the dinuclearity and composition during catalysis, with acetate bound as a terminal ligand.

The fact that **1** dismutates H_2O_2 at a constant rate upon successive additions of H_2O_2 to the buffered solution of the complex confirms that the starting complex is the true catalyst. Kinetic results show that complex **1** catalyzes the dismutation of H_2O_2 with saturation kinetics on the substrate, first order dependence on the catalyst, and $k_{cat}/K_M = 16(1) \times 10^2$ s^{-1} M^{-1}, at pH 10.6. On the basis of the k_{cat}/K_M criterion, complex **1** is the most efficient model known to date, and this is the consequence of its high affinity for the substrate. The K_M value of 6.6 mM determined for complex **1** is lower than the K_M of 15, 83, and 350 mM of MnCAT from *T. album*,[55] *T. thermophilus*,[56] and *L. plantarum*,[57] respectively. Thus, the catalytic efficiency (k_{cat}/K_M) of **1** is only 60 times lower than MnCAT from *L. plantarum* and 2 × 10^3 times lower than that of *T. thermophilus*, the most efficient MnCAT.[57,58]

The CAT activity and the substrate affinity of **1** are highly sensitive to pH. In unbuffered solutions of protic solvents, the complex gradually loses activity with the formation of an inactive Mn^{II} species. At neutral pH, complex **1** is more than two-times less efficient than at pH 10.6. The pH dependence of the activity and K_M shown by complex **1** parallels the behavior of Y42F LPC, a mutant of *L. plantarum* catalase, where Tyr42 has been replaced by phenylalanine.[58] This mutant has less than 5% of the wild type MnCAT activity at neutral pH and a much higher K_M for H_2O_2 (≈ 1.4 M) at neutral pH than at pH 10 (K_M 220 mM). In the wild type enzyme, Tyr42 is involved in a web of hydrogen bonds that contributes to stabilize the diMn core with a pair of solvent bridges. As a consequence, although presenting the highest

dx.doi.org/10.1021/ic2011452 |*Inorg. Chem.* 2011, 50, 8973–8983

activity between pH 8 and 10, MnCATs are active over a wide pH range of 5 to 12.[59] Replacement of Tyr42 residue disrupts the hydrogen-bonded web, the double solvent bridged diMn core is not further stabilized, and efficient CAT activity and substrate affinity are only achieved at high pH. In the case of **1**, protonation of the bridging ligands modifies the redox and coordination properties of the diMn core, causing the gradual loss of activity as the pH decreases. The exogenous base contributes to retain the integrity of the double bridged diMn core and favors the formation of the catalyst-peroxide adduct, rendering **1** a highly efficient catalyst for H_2O_2 disproportionation.

■ ASSOCIATED CONTENT

Supporting Information. X-ray crystallographic file in CIF format for the structure determination of complex **1**-(MeOH), a stereoview of compound **1**(MeOH) showing intermolecular Na-bonding, RR spectra of reaction mixtures, and scheme of ligands mentioned in the text. This material is available free of charge via the Internet at http://pubs.acs.org.

■ AUTHOR INFORMATION

Corresponding Author
*E-mail: signorella@iquir-conicet.gov.ar.

■ ACKNOWLEDGMENT

We thank the National University of Rosario, CONICET, and the National Agency for Sciences Promotion for financial support and M. De Gaudio for volumetric measurements.

■ REFERENCES

(1) (a) Bravo, J.; Mate, M. J.; Schneider, T.; Switala, J.; Wilson, K.; Loewen, P. C.; Fita, L. *Proteins Struct., Funct., Bioinf.* **1999**, *34*, 155–166. (b) Riggs-Gelasco, P. J.; Mei, R.; Penner-Hahn, J. E. In *Mechanistic Bioinorganic Chemistry*; Thorp, H. H., Pecoraro, V. L., Eds.; American Chemical Society: Washington, DC, 1995; Ch 8.

(2) Sayre, L. M.; Perry, G.; Smith, M. A. *Chem. Res. Toxicol.* **2008**, *21*, 172–188.

(3) (a) Day, B. J. *Biochem. Pharmacol.* **2009**, *77*, 285–296. (b) Hanawa, T.; Asayama, S.; Watanabe, T.; Owada, S.; Kawakamai, H. *J. Controlled Release* **2009**, *135*, 60–64.

(4) (a) Brazier, M. W.; Doctrow, S. R.; Masters, C. L.; Collins, S. J. *Free Radical Biol. Med.* **2008**, *45*, 184–192. (b) Day, B. J. *Drug Discovery Today* **2004**, *9*, 557–566. (c) McDonald, M. C.; di Villa Bianca, R. E.; Wayman, N. S.; Pinto, A.; Sharpe, M. A.; Cuzzocrea, S.; Chatterjee, P. K.; Thiemermann, C. *Eur. J. Pharmacol.* **2003**, *466*, 181–189.

(5) (a) Antonyuk, S. V.; Melik-Adamyan, V. R.; Popov, A. N.; Lamzin, V. S.; Hempstead, P. D.; Harrison, P. M.; Artymiuk, P. J.; Barynin, V. V. *Crystallogr. Rep.* **2000**, *45*, 105–116. (b) Barynin, V. V.; Whittaker, M. M.; Antonyuk, S. V.; Lamzin, V. S.; Harrison, P. M.; Artymiuk, P. J.; Whittaker, J. W. *Structure* **2001**, *9*, 725–738.

(6) Wu, A. J.; Penner-Hahn, J. E.; Pecoraro, V. L. *Chem. Rev.* **2004**, *104*, 903–938.

(7) Dubois, L.; Xiang, D. F.; Tan, X. S.; Latour, J. M. *Eur. J. Inorg. Chem.* **2005**, 1565–1571.

(8) De Boer, J. W.; Browne, W. R.; Feringa, B. L.; Hage, R. *C. R. Chim.* **2007**, *10*, 341–354.

(9) Signorella, S.; Tuchagues, J. P.; Moreno, D.; Palopoli, C. In *Inorganic Biochemistry Research Progress*; Hughes, J. G., Robinson, A. J., Eds.; Nova Science Publishers Inc.: New York, 2008; pp 243−279.

(10) Berben, L. A.; Peters, J. C. *Inorg. Chem.* **2008**, *47*, 11669–11679.

(11) Kaizer, J.; Csonka, R.; Speier, G. *React. Kinet. Catal. Lett.* **2008**, *94*, 157–163.

(12) Dubois, L.; Pécaut, J.; Charlot, M. F.; Baffert, C.; Collomb, M. N.; Deronzier, A.; Latour, J. M. *Chem.—Eur. J.* **2008**, *14*, 3013–3025.

(13) Jiang, X.; Liu, H.; Zheng, B.; Zhang, J. *Dalton Trans.* **2009**, 8714–8723.

(14) Berggren, G.; Huang, P.; Eriksson, L.; Styring, S.; Anderlund, M. F.; Thapper, A. *Dalton Trans.* **2010**, 11035–11044.

(15) Shin, B. K.; Kim, M.; Han, J. *Polyhedron* **2010**, *29*, 2560–2568.

(16) Lessa, J. A.; Horn, A., Jr.; Bull, E. S.; Rocha, M. R.; Benassi, M.; Catharino, R. R.; Eberlin, M. N.; Casellato, A.; Noble, C. J.; Hanson, G. R.; Schenk, G.; Silva, G. C.; Antunes, O. A. C.; Fernandes, C. *Inorg. Chem.* **2009**, *48*, 4569–4579.

(17) Doctrow, S. R.; Huffman, K.; Marcus, C. B.; Tocco, G.; Malfroy, E.; Adinolfi, C. A.; Kruk, H.; Baker, K.; Lazarowych, N.; Mascarenhas, J.; Malfroy, B. *J. Med. Chem.* **2002**, *45*, 4549–4558.

(18) Nishida, Y.; Akamatsu, T.; Tsuchiya, K.; Sakamoto, M. *Polyhedron* **1994**, *13*, 2251–2254.

(19) Kani, I.; Darak, C.; Sahin, O.; Büyükgüngör, O. *Polyhedron* **2008**, *27*, 1238–1247.

(20) (a) Berry, K. J.; Moya, F.; Murray, K. S.; v. d. Bergen, A. M. B.; West, B. O. *J. Chem. Soc., Dalton Trans.* **1982**, 109–116. (b) Botsivali, M.; Evans, D. F.; Missen, P. H.; Upton, M. W. *J. Chem. Soc., Dalton Trans.* **1985**, 1147–1149.

(21) Murase, I.; Hatano, M.; Tanaka, M.; Ueno, S.; Okawa, H.; Kida, S. *Bull. Chem. Soc. Jpn.* **1982**, *55*, 2404–2408.

(22) Palopoli, C.; Chansou, B.; Tuchagues, J. P.; Signorella, S. *Inorg. Chem.* **2000**, *39*, 1458–1462.

(23) *CrysAlis Pro*, version 1.171.33.66; Oxford Diffraction Ltd.: Oxford, U.K., 2010.

(24) Altomare, A.; Cascarano, G.; Giacovazzo, C.; Guagliardi, A. *J. Appl. Crystallogr.* **1993**, *26*, 343–350.

(25) Sheldrick, G. M. *SHELXL-97, Program for Crystal Structure Refinement*; University of Göttingen: Göttingen, Germany, 1997.

(26) Walker, N.; Stuart, D. *Acta Crystallogr., Sect. A* **1983**, *39*, 158.

(27) Watkin, D. J.; Prout, C. K.; Pearce, L. J. *CAMERON*, Chemical Crystallography Laboratory, Oxford, UK, 1996.

(28) Spek, A. L. *Acta Crystallogr., Sect. A* **1990**, *46*, C34.

(29) (a) Deacon, G. B.; Phillips, R. J. *Coord. Chem. Rev.* **1980**, *33*, 227–250.(b) Nakamoto, K. *Infrared and Raman Spectra of Inorganic and Coordination Compounds*, 5th ed.; Wiley-Interscience: New York, 1997; Part B, p 60.

(30) (a) Biava, H.; Palopoli, C.; Shova, S.; De Gaudio, M.; Daier, V.; González-Sierra, M.; Tuchagues, J. P.; Signorella, S. *J. Inorg. Biochem.* **2006**, *100*, 1660–1671. (b) Moreno, D.; Palopoli, C.; Daier, V.; Shova, S.; Vendier, L.; González Sierra, M.; Tuchagues, J. P.; Signorella, S. *Dalton Trans.* **2006**, 5156–5166. (c) Daier, V.; Biava, H.; Palopoli, C.; Shova, S.; Tuchagues, J. P.; Signorella, S. *J. Inorg. Biochem.* **2004**, *98*, 1806–1817. (d) Palopoli, C.; González-Sierra, M.; Robles, G.; Dahan, F.; Tuchagues, J. P.; Signorella, S. *J. Chem. Soc., Dalton Trans.* **2002**, 3813–3819.

(31) Gelasco, A.; Pecoraro, V. L. *J. Am. Chem. Soc.* **1993**, *115*, 7928–7929.

(32) Gelasco, A.; Kirk, M. L.; Kampf, J. W.; Pecoraro, V. L. *Inorg. Chem.* **1997**, *36*, 1829–1837.

(33) Bertoncello, K.; Fallon, G. D.; Murray, K. S.; Tiekink, E. R. T. *Inorg. Chem.* **1991**, *30*, 3562–3568.

(34) Mikuriya, M.; Yamato, Y.; Tokii, T. *Bull. Chem. Soc. Jpn.* **1992**, *65*, 1466–1468.

(35) Biava, H.; Palopoli, C.; Duhayon, C.; Tuchagues, J.-P.; Signorella, S. *Inorg. Chem.* **2009**, *48*, 3205–3214.

(36) Zhang, Z.; Brouca-Cabarrecq, C.; Hemmert, C.; Dahan, F.; Tuchagues, J.-P. *J. Chem. Soc., Dalton Trans.* **1995**, 1453–1460.

(37) Zhang, J. J.; Luo, Q. H.; Duan, C. Y.; Wang, Z. L.; Mei, Y. H. *J. Inorg. Biochem.* **2001**, *86*, 573–579.

(38) Miyasaka, H.; Clérac, R.; Wernsdorfer, W.; Lecren, L.; Bonhomme, C.; Sugiura, K. I.; Yamashita, M. *Angew. Chem., Int. Ed.* **2004**, *43*, 2801–2805.

(39) Dubois, L.; Xiang, D. F.; Tan, X. S.; Pécaut, J.; Jones, P.; Baudron, S.; Le Pape, L.; Latour, J. M.; Baffert, C.; Chardon-Noblat, S.; Collomb, M. N.; Deronzier, A. *Inorg. Chem.* **2003**, *42*, 750–760.

(40) Karsten, P.; Neves, A.; Bortoluzzi, A. J.; Strähle, J.; Maichle-Mössmer, C. *Inorg. Chem. Commun.* **2002**, *5*, 434–438.
(41) Sabater, L.; Hureau, C.; Blain, G.; Guillot, R.; Thuéry, P.; Rivière, E.; Aukauloo, A. *Eur. J. Inorg. Chem.* **2006**, 4324–4337.
(42) Hureau, C.; Sabater, L.; Gonnet, F.; Blain, G.; Sainton, J.; Anxolabéhère-Mallart, E. *Inorg. Chim. Acta* **2006**, *359*, 339–345.
(43) (a) Bonadies, J.; Maroney, M. J.; Pecoraro, V. L. *Inorg. Chem.* **1989**, *28*, 2044–2051. (b) Caudle, M. T.; Riggs-Gelasco, P.; Gelasco, A. K.; Penner-Hahn, J. E.; Pecoraro, V. L. *Inorg. Chem.* **1996**, *35*, 3577–3584. (c) Bermejo, M. R.; González, A. M.; Fondo, M.; García-Deibe, A.; Maneiro, M.; Sanmartín, J.; Hoyos, O. L.; Watkinson, M. *New J. Chem.* **2000**, *24*, 235–241. (d) Bermejo, M. R.; González-Noya, A. M.; Abad, V.; Fernández, M. I.; Maneiro, M.; Pedrido, R.; Vásquez, M. *Eur. J. Inorg. Chem.* **2004**, 3696–3705.
(44) (a) Boelrijk, A. E. M.; Khangulov, S. V.; Dismukes, G. C. *Inorg. Chem.* **2000**, *39*, 3009–3019. (b) Larson, E. J.; Pecoraro, V. L. *J. Am. Chem. Soc.* **1991**, *113*, 7809–7810. (c) Bonadies, J. A.; Kirk, M. L.; Lah, M. S.; Kessissoglou, D. P.; Hatfield, W. E.; Pecoraro, V. L. *Inorg. Chem.* **1989**, *28*, 2037–2044. (d) Larson, E. J.; Pecoraro, V. L. *J. Am. Chem. Soc.* **1991**, *113*, 3810–3818.
(45) (a) Hureau, C.; Sabater, L.; Anxolabéhère-Mallart, E.; Nierlich, M.; Charlot, M.-F.; Gonnet, F.; Rivière, E.; Blondin, G. *Chem.—Eur. J.* **2004**, *10*, 1998–2010. (b) Baldwin, M. J.; Pecoraro, V. L. *J. Am. Chem. Soc.* **1996**, *118*, 11325–11326.
(46) (a) Schardt, B. C.; Hollander, F. J.; Hill, C. L. *J. Am. Chem. Soc.* **1982**, *104*, 3964–3972. (b) Czernuszewicz, R. S.; Su, Y. O.; Stern, M. K.; Macor, K. A.; Kim, D.; Groves, J. T.; Spiro, T.G. *J. Am. Chem. Soc.* **1988**, *110*, 4158–4165. (c) Groves, J. T.; Stern, M. K. *J. Am. Chem. Soc.* **1988**, *110*, 8628–8638.
(47) Song, W. J.; Seo, M. S.; George, S. D.; Ohta, T.; Song, R.; Kang, M. J.; Tosha, T.; Kitagawa, T.; Solomon, E. I.; Nam, W. *J. Am. Chem. Soc.* **2007**, *129*, 1268–1277.
(48) (a) Sakiyama, H.; Tamaki, H.; Kodera, M.; Matsumoto, N.; Okawa, H. *J. Chem. Soc., Dalton Trans.* **1993**, 591–595. (b) Sakiyama, H.; Okawa, H.; Isobe, R. *J. Chem. Soc., Chem. Commun.* **1993**, 882–884. (c) Higuchi, C.; Sakiyama, H.; Okawa, H.; Fenton, D. E. *J. Chem. Soc., Dalton Trans.* **1995**, 4015–4020. (d) Itoh, M.; Motoda, K.; Shindo, K.; Kamiusuki, T.; Sakiyama, H.; Matsumoto, N.; Okawa, H. *J. Chem. Soc., Dalton Trans.* **1995**, 3635–3641. (e) Aono, T.; Wada, H.; Yonemura, M.; Ohba, M.; Okawa, H.; Fenton, D. E. *J. Chem. Soc., Dalton Trans.* **1997**, 1527–1531.
(49) Gelasco, A.; Bensiek, S.; Pecoraro, V. L. *Inorg. Chem.* **1998**, *37*, 3301–3309.
(50) Boelrijk, A. E. M.; Dismukes, G. C. *Inorg. Chem.* **2000**, *39*, 3020–3028.
(51) Triller, M. U.; Hsieh, W. Y.; Pecoraro, V. L.; Rompel, A.; Krebs, B. *Inorg. Chem.* **2002**, *41*, 5544–5554.
(52) Signorella, S.; Rompel, A.; Buldt-Karentzopoulos, K.; Krebs, B.; Pecoraro, V. L.; Tuchagues, J.-P. *Inorg. Chem.* **2007**, *46*, 10864–10868.
(53) Godbole, M. D.; Kloskowski, M.; Hage, R.; Rompel, A.; Mills, A. M.; Spek, A. L.; Bouwman, E. *Eur. J. Inorg. Chem.* **2005**, 305–313.
(54) Shorter, J. *Correlation Analysis of Organic Reactivity*; Research Studies Press: New York, 1983; pp 146−153.
(55) Penner-Hahn, J. E.; Pecoraro, V. L. In *Manganese Redox Enzymes*; Pecoraro, V. L., Ed.; VCH: New York, 1992; pp 29, 197.
(56) Shank, M.; Barynin, V.; Dismukes, G. C. *Biochemistry* **1994**, *33*, 15433–15436.
(57) Penner-Hahn, J. E. In *Manganese Redox Enzymes*; Pecoraro, V. L., Ed.; VCH: New York, 1992; pp 29−45.
(58) Whittaker, M. M.; Barynin, V. V.; Igarashi, T.; Whittaker, J. W. *Eur. J. Biochem.* **2003**, *270*, 1102–1116.
(59) (a) Amo, T.; Atomi, H.; Imanaka, T. *J. Bacteriol.* **2002**, *184*, 3305–3312. (b) Allgood, G. S.; Perry, J. J. *J. Bacteriol.* **1986**, *168*, 563–567. (c) Kagawa, M.; Murakoshi, N.; Nishikawa, Y.; Matsumoto, G.; Kurata, Y.; Mizobata, T.; Kawata, Y.; Nagai, J. *Arch. Biochem. Biophys.* **1999**, *362*, 346–355.